International Journal of Power Electronics and Drive System (IJPEDS)
Vol. 17, No. 4, December 2026, pp. 2612~2629
ISSN: 2088-8694, DOI: 10.11591/ijpeds.v17.i4.pp2612-2629

Nonlinear wheeled vehicle lateral stability enhancement using extended Kalman filter and adaptive model predictive control

Fatima-Zahra Rahmouni, Mohammed Bakhti
École Nationale Supérieure d'Arts et Métiers, Moulay Ismail University, Meknes, Morocco

Article Info

Article history:

Received Apr 19, 2026
Revised Sep 12, 2026
Accepted Sep 17, 2026

Keywords:

Adaptive model predictive control
Extended Kalman filter
Nonlinear tire model
Vehicle dynamics
Vehicle lateral stability

ABSTRACT

This study assesses control performance and steering precision for wheeled vehicles using a nested-loop strategy that integrates an adaptive model predictive control (MPC) (outer loop) with extended Kalman filter (EKF)-based state estimation and a BLDC-driven steering actuator regulated by a state-space PI controller (inner loop). Distinct from prior MPC–Kalman approaches focused solely on vehicle states, our design explicitly co-models and closes the loop around the BLDC steering drive, thus bridging vehicle dynamics and drive-system actuation within one predictive framework. The inner loop targets a brushless DC (BLDC) motor as steering actuator with a proportional integral (PI) controller, while the outer control layer generates the driver reference steering angle by combining predictive control with state estimation. The simulation scenario considers simultaneously noisy measurements and control signal disturbances to emulate real driving conditions, and it is conducted to appraise the control strategy efficiency and robustness based on an accurate nonlinear tire-road model.

This is an open access article under the CC BY-SA license.

Corresponding Author:

Fatima-Zahra Rahmouni
Ecole Nationale Supérieure d'Arts et Métiers, Moulay Ismail University
Meknes, Morocco
Email: f.rahmouni@edu.umi.ac.ma

1. INTRODUCTION

The integration of high-performance power electronics with sophisticated electric drive control algorithms has become a key enabler of recent developments in advanced driver assistance systems (ADAS). As automotive architectures transition toward full electrification, the effectiveness of autonomous control functions is increasingly defined by the precision of power conversion stages and the dynamic response of the underlying motor drive systems [1]. In this context, the shift from conventional mechanical linkages to electronic actuation in steering subsystems is paramount, requiring robust motor control strategies to ensure optimal lateral stability and maneuverability under diverse operating conditions. Recent developments in vehicle chassis control have shown a growing trend toward electrically actuated and distributed architectures integrating steering, braking, and propulsion systems to enhance overall vehicle dynamics and safety [2]. Furthermore, the integration of these electrified modules necessitates the implementation of stringent functional safety standards, such as ISO 26262, to mitigate risks associated with electronic hardware failures [3].

In modern electric and autonomous vehicles, steer-by-wire architectures actuated by BLDC motors are increasingly adopted due to their high efficiency, fast dynamic response, reduced maintenance requirements, and compatibility with electronic drive systems. Unlike hydraulic steering, steer-by-wire removes the direct mechanical link between the road wheels and the steering wheel, which opens the door to more advanced control functions and greater design freedom [4]. These characteristics make BLDC-actuated steer-by-wire systems suitable for integration with advanced vehicle-level control strategies, where accurate and rapid steering actuation is essential for maintaining lateral stability and trajectory-tracking performance.

Furthermore, BLDC-based steering actuators require the coordinated design of power electronics, motor drive control, and vehicle-level control algorithms [5]. Consequently, steering performance depends not only on vehicle dynamics but also on the electrical and mechanical behavior of the actuator drive system. Therefore, considering the actuator dynamics together with the vehicle model is important when evaluating the overall performance of advanced steering-control architectures.

To mitigate these challenges, numerous control strategies have been reported in the literature. Among them, model predictive control (MPC) has appeared as a promising solution for vehicle lateral control because of its capability to effectively manage multivariable systems, operational constraints, and future system behavior over a prediction horizon. Recent studies have successfully applied nonlinear MPC approaches to improve vehicle stability and maximize tire force usage under demanding driving conditions [6], [7]. In parallel, classical state-feedback methods based on pole placement continue to be widely employed for steering actuator control due to their simplicity, stability properties, and satisfactory tracking performance [8].

Accurate state information is equally important for achieving satisfactory vehicle control performance. Since vehicle lateral velocity and yaw rate measurements are often corrupted by sensor noise and disturbances, state estimation techniques have received considerable attention. Kalman filter (KF)-based approaches and their nonlinear extensions, particularly the extended Kalman filter (EKF), have been extensively applied in automotive systems to estimate vehicle states and improve robustness against measurement uncertainties [9], [10]. Other observer-based methods have also been investigated to enhance estimation accuracy and system reliability under uncertain operating conditions [11].

Despite the significant progress achieved in vehicle lateral control and state estimation, several limitations remain in the existing literature. Many studies focus exclusively on vehicle-level controllers while assuming ideal steering actuation systems [12]. Conversely, investigations dedicated to steering actuator control often neglect the interaction between actuator dynamics and vehicle lateral dynamics. Moreover, the combined effects of actuator disturbances, model uncertainties, and noisy measurements are rarely addressed within a unified control framework. As a result, the influence of brushless direct current (BLDC) steering actuator dynamics on the performance and robustness of advanced vehicle-level controllers remains insufficiently investigated.

To overcome these limitations, this paper suggests a nested-loop control architecture for nonlinear vehicle lateral stability enhancement. The outer loop employs an adaptive model predictive controller (AMPC) to generate steering angle references based on a nonlinear bicycle vehicle model linearized online through Jacobian evaluation. The inner loop consists of a BLDC steering actuator regulated by a state-space proportional-integral (PI) controller designed using pole-placement techniques. In addition, an EKF is integrated into the control structure to estimate vehicle states in noisy measurement environment and control signal disturbances. The proposed control scheme is tested with a nonlinear Pacejka tire model on single lane change (SLC) and double lane change (DLC) maneuvers implemented using MATLAB/Simulink.

The significance of this work lies in the integration of adaptive predictive control, nonlinear vehicle dynamics, BLDC steering actuator dynamics, and Kalman-filter-based state estimation within a unified framework. The obtained results validate the proposed control strategy ability to maintain accurate tracking and robust vehicle lateral stability under realistic operating conditions involving actuator disturbances, parameter uncertainties, and noisy measurements. Consequently, the proposed methodology constitutes a relevant contribution to the evolution of advanced steering control technologies for future electric as well as autonomous vehicles. The remainder of this paper is organized as follows: i) Section 2 introduces the adopted single-track vehicle representation along with the tire–road friction formulation used; ii) Section 3 covers the nonlinear model linearization, the AMPC design, the steering-subsystem control law, and the EKF algorithm; iii) Section 4 discusses the simulation outcomes; whereas iv) Section 5 summarizes the principal findings of the study.

2. METHOD

This study builds and validates a lateral-stability control strategy for the vehicle, relying on simulation as the main evaluation tool. This approach is suitable as it enables systematic analysis of nonlinear vehicle dynamics and actuator behavior under controlled and reproducible conditions, including measurement noise and external disturbances. This section presents the mathematical modeling of the vehicle and steering actuator, followed by the design of the control and estimation strategies used in this work.

2.1. Lateral vehicle dynamics and tire model

The control architecture relies on a vehicle lateral behavior's mathematical representation together with the steering actuator dynamics. A reliable system model is required to examine the interaction between these components and to assess the proposed control approach through numerical simulations. Accordingly, the vehicle lateral dynamics are formulated using a nonlinear Pacejka tire–road interaction model. For the

steering-by-wire system, the actuator is represented by a BLDC motor to obtain a tractable model. The resulting formulation provides the basis for analyzing the vehicle response and evaluating the stability characteristics associated with the considered electric vehicle platform [13].

The vehicle dynamics are represented using a simplified yet highly accurate single-track model, commonly termed the bicycle model. The front and rear wheel pairs are replaced by equivalent wheels located on their respective axles, with the resulting configuration depicted in Figure 1. This representation reduces the model complexity while retaining the principal lateral and yaw dynamics required for the design and evaluation of the proposed lateral stability controller.

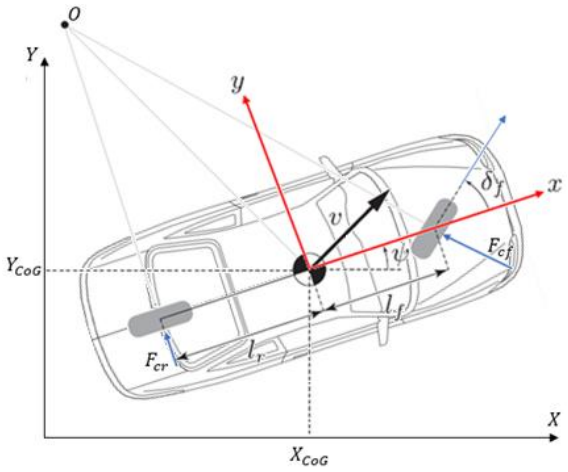

Figure 1. Vehicle model based on a single-track representation

Applying Newton's second law gives the following expression for the vehicle's lateral dynamics [14]:

$$ma_y = 2\left(F_{cf}\cos\left(\delta_f\right) + F_{cr}\right) \quad (1)$$

where a_y is the lateral vehicle center of gravity acceleration, and F_{cf} and F_{cr} intend to lateral lateral forces generated at the front and rear tires respectively. Let v_x be the vehicle longitudinal speed and ψ be its yaw angle. Both the acceleration $\dot{y}$ among the lateral-acceleration component and the centripetal term n $v_x\dot{\psi}$ contribute to a_y as (2).

$$a_y = \frac{dv_y}{dt} + v_x\dot{\psi} \quad (2)$$

Subsequently, the dynamic equation of the vehicle along the y axis is given by (3).

$$\frac{dv_y}{dt} = -v_x\dot{\psi} + \frac{2}{m}\left(F_{cf}\cos\left(\delta_f\right) + F_{cr}\right) \quad (3)$$

The yaw-rate $\dot{\psi}$ dynamics follow from the vehicle moment equilibrium and are expressed as (4).

$$\frac{d\dot{\psi}}{dt} = \frac{l_f F_{cf} - l_r F_{cr}}{I_z} \quad (4)$$

Where δ_f implies the front wheel steering angle, while l_f and l_r represent the distances from the vehicle center of gravity to the front and rear axles, respectively. The parameter I_z is the vehicle moment of inertia around the vertical axis. For accuracy, the nonlinear lateral tire forces are computed from Pacejka's magic formula tire model [15]. The forces are related to front and rear tire slip angles as (5) and (6).

$$F_{cf} = -\mu F_{zf}\, sin\left(C\ atan\left(B\ \alpha_f - E\left(B\ \alpha_f - \text{atan}\left(\alpha_f\right)\right)\right)\right) \quad (5)$$

$$F_{cr} = -\mu F_{zr}\, sin\left(C\ atan\left(B\ \alpha_r - E(B\ \alpha_r - \text{atan}(\alpha_r))\right)\right) \quad (6)$$

Where μ refers to the friction coefficient at the tire–road interface, and B designates the stiffness factor:

B =$C_{\text{F}\alpha}$ /(CD)

With the cornering stiffness: $C_{\text{F}\alpha}$= c_1 sin {2 arctan (Fz /c_2)}.

The parameters C, E, c_1, c_2 and the friction coefficient μ, which may vary with vertical load and vehicle speed, can be identified using regression-based methods. Figure 2 illustrates the variation in lateral force with respect to the slip angle, highlighting the nonlinear behavior and saturation effects captured by the Pacejka model.

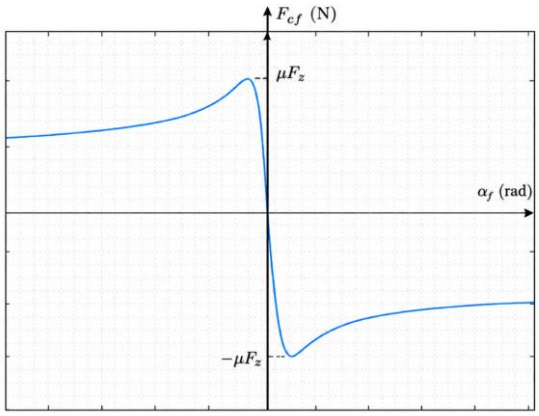

Figure 2. Tire slip angle and lateral force at the front tire

In this paper, normal loads on the wheels at the front and rear axles F_{zf} and F_{zr} are not relying on the longitudinal acceleration. This assumption is quite practical to simplify the vehicle dynamics equation. Thus, they are given by (7) and (8).

$$F_{zf} = \frac{mgl_f}{l_f+l_r} \quad (7)$$

$$F_{zr} = \frac{mgl_r}{l_f+l_r} \quad (8)$$

Where m denotes the vehicle mass, while g represents the gravitational acceleration.

According to [14], and as depicted in Figure 3, the slip angles corresponding to the front and rear wheels are respectively (9) and (10).

$$\alpha_f = \frac{(v_y+\dot{\psi}l_f)cos(\delta_f)-v_x sin(\delta_f)}{(v_y+\dot{\psi}l_f)sin(\delta_f)+v_x cos(\delta_f)} \quad (9)$$

$$\alpha_r = \frac{(v_y-\dot{\psi}l_r)}{v_x} \quad (10)$$

Both electrical and mechanical equations describe the behavior of the brushless DC (BLDC) motor that drives the steering subsystem [16]. The dynamic equation of the phase current is given by (11).

$$\frac{di}{dt} = \frac{\alpha V_{dc}-2Ri-2K_e\omega_M}{2L} \quad (11)$$

In (11), α is the control duty cycle, and V_{dc} is the DC bus voltage. The equivalent resistance and inductance of the two conductive phases are $2R$ and $2L$ respectively, and the back counter-electromotive force (EMF) term is $2K_e\omega_M$, where K_e and ω_M are a motor constant and the motor shaft rotational speed.

The electromagnetic torque of the BLDC is (12).

$$T_e = K_t i \tag{12}$$

To complete the mathematical model of the steering subsystem, the mechanical dynamics of the actuator is incorporated as (13).

$$\frac{d\omega_M}{dt} = \frac{1}{J}(T_e - B\omega_M) = \frac{1}{J}(K_t i - B\omega_M) \tag{13}$$

In this model, B and J designate the equivalent viscous friction coefficient and the equivalent steering-subsystem moment of inertia, respectively. The rack-and-pinion transmission links the motor shaft angle θ_M to the front-wheel steering angle δ_f through the gear ratio r, yielding (14).

$$\delta_f = r\theta_M \tag{14}$$

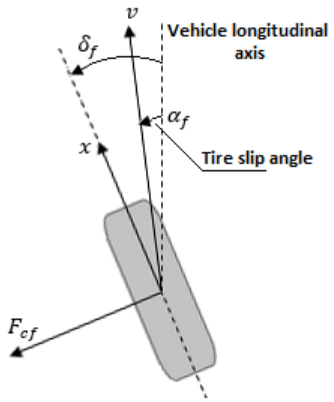

Figure 3. Pacejka tire model (front wheel)

2.2. State space model formulation

Combining (1) to (10) and letting $x = [x_1, x_2]^{\mathrm{T}} = [v_y, \dot{\psi}]^{\mathrm{T}} \in \mathbb{R}^2$ and $u(t) = \delta_f$, we get the nonlinear state space model for the vehicle lateral dynamics (15).

$$\dot{x} = f(x, u) \tag{15}$$

The vector-valued functions $f(.)$ is defined as (16).

$$f(x,u) = \begin{pmatrix} -v_x\dot{\psi} + \frac{2}{m}\left(F_{cf}\cos(\delta_f) + F_{cr}\right) \\ \frac{l_f F_{cf} - l_r F_{cr}}{I_z} \end{pmatrix} = \begin{pmatrix} f_1(x,u) \\ f_2(x,u) \end{pmatrix} \tag{16}$$

Based on (11) to (14), and letting $x = [x_1, x_2]^{\mathrm{T}} = [i, \omega_M]^{\mathrm{T}} \in \mathbb{R}^2$ and $u(t) = \alpha$, we get the linear state space model for the steering subsystem:

$$\dot{x} = Ax + Bu \tag{17}$$

Where constant matrices A and B are given by (18) and (19).

$$A = \begin{bmatrix} -\frac{R}{L} & -\frac{K_e}{L} \\ \frac{K_t}{J} & \frac{-B}{J} \end{bmatrix} \tag{18}$$

$$B = \begin{bmatrix} \frac{V_{dc}}{2L} \\ 0 \end{bmatrix} \tag{19}$$

3. PROPOSED CONTROL METHOD

The proposed control strategy is implemented following a structured procedure, including model linearization, controller design, state estimation, and system integration. The proposed AMPC controller aims to track the vehicle's lateral speed v_y and its angular velocity around the vertical axis $\dot{\psi}$. The front steering angle δ_f serves as the system control input, and a similar vehicle model is used to constantly supply the targeted state references v_{yref} and $\dot{\psi}_{ref}$.

State feedback required by the AMPC controller is fed back using an EKF. In this paper, it is assumed that the vehicle lateral velocity v_y and yaw rate $\dot{\psi}$ constitute the measured outputs, yet they are affected by a Gaussian white measurement noise of constant covariance matrix. The measurement-noise model is introduced to reproduce realistic sensing conditions and to evaluate the ability of the EKF to reconstruct reliable vehicle states for feedback control.

The control signal derived by the AMPC controller is fed to a state-space proportional-integral (PI) controller, which is the lower-level steering angle tracking controller. Gaussian white control noise is also affects the applied steering angle supplied by the steering actuator subsystem. In this paper, the front and rear wheels' tire-road friction coefficient μ is considered known. All the assumptions are reasonable as the lateral vehicle speed and yaw rate are available in commercial cars equipped with electronic stability program (ESP) or measurement unit (IMU) [17]-[19], and the tire-road friction coefficient can be determined through measurement or estimation techniques, as described in [20], [21]. The proposed approach involves the following main steps:

3.1. Model linearization

Jacobian matrices of the adopted single-track representation, described by (15) and (16), is required by both the AMPC and the EKF algorithms. Its expression is depicted by (20) and (21).

$$A_v = \begin{pmatrix} \left.\frac{df_1}{dx_1}\right|_{x_0,u_0} & \left.\frac{df_1}{dx_2}\right|_{x_0,u_0} \\ \left.\frac{df_2}{dx_1}\right|_{x_0,u_0} & \left.\frac{df_2}{dx_2}\right|_{x_0,u_0} \end{pmatrix} \tag{20}$$

$$B_v = \begin{pmatrix} \left.\frac{df_1}{du}\right|_{x_0,u_0} \\ \left.\frac{df_2}{du}\right|_{x_0,u_0} \end{pmatrix} \tag{21}$$

Where x_0 and u_0 are the actual system state trajectory and actual input evaluated reiteratively. The output matrix C is the identity as $y(k) = x(k)$.

Since both the AMPC and the Extended Kalman Filter (EKF) are implemented in discrete time domain, the linearized continuous-time model is converted to discrete time using a sampling period T_s. The resulting discrete state-space representation is then employed for the controller design and state estimation. Using the Jacobian matrices defined in (20) and (21), the state derivative can be approximated as:

$$\dot{x}(t) \approx [x(t+T_s) - x(t)] / T_s$$

substituting this approximation into the linearized state equation yields:

$$x(t+T_s) = (I + A_v\, T_s)x(t) + B_v\, T_s u(t)$$

considering system at the sampling instants t = kT_s, the corresponding discrete-time model is formulated as:

$$x(k+1) = A_{vd}\, x(k) + B_{vd}\, u(k)$$
$$y(k) = C_d x(k)$$

where:

$$A_{vd} = I + A_v T_s$$
$$B_{vd} = B_v T_s$$
$$C_d = C$$

the obtained discrete-time matrices are subsequently employed to construct the augmented prediction AMPC model and EKF state-prediction model.

3.2. Upper-level AMPC controller formulation

Using the system Jacobian matrices, the incremental state-feedback law for the AMPC scheme is formulated within a state-space framework as (22) [22].

$$\Delta u(k) = u(k+1) - u(k) = K_r r(k) - K_x x(k) \tag{22}$$

Where $r(k)$ is the reference vector $[v_{yref}, \dot{\psi}_{ref}]^{\mathrm{T}} \in \mathbb{R}^2$ and time-varying matrices K_r and K_x are given as (23) and (24).

$$K_r = \left[[1 \quad 0 \quad 0 \quad \ldots \quad 0]_{1\times N_c}(\Phi^{\mathrm{T}}\Phi + R)^{-1}\Phi^{\mathrm{T}}Q\overline{S_p}\right] \tag{23}$$

$$K_x = \left[[1 \quad 0 \quad 0 \quad \ldots \quad 0]_{1\times N_c}(\Phi^{\mathrm{T}}\Phi + R)^{-1}\Phi^{\mathrm{T}}QF\right] \tag{24}$$

Where:

$$\Phi = \begin{bmatrix} C_aB_a & 0 & 0 & \ldots & 0 \\ C_aA_aB_a & C_aB_a & 0 & \ldots & 0 \\ C_aA_a^2B_a & C_aA_aB_a & C_aB_a & \ldots & 0 \\ \ldots & \ldots & \ldots & \ldots & \ldots \\ \ldots & \ldots & \ldots & \ldots & \ldots \\ C_aA_a^{N_p-1}B_a & C_aA_a^{N_p-2}B_a & C_aA_a^{N_p-3}B_a & \ldots & C_aA_a^{N_p-N_c}B_a \end{bmatrix} \tag{25}$$

$$F = \begin{bmatrix} C_aA_a & C_aA_a^2 & C_aA_a^3 \ldots & C_aA_a^{N_p} \end{bmatrix}^T \tag{26}$$

$$S_p = [1 \quad 1 \quad \ldots \quad 1]_{1\times N_p} r(k) = \overline{S_p} r(k) \tag{27}$$

Tuning parameters N_p and N_c are respectively the prediction and control horizons. Augmented state matrices of the system are given by (28)-(30).

$$A_a = \begin{bmatrix} A_{vd} & 0_{2\times 2} \\ CA_{vd} & \mathrm{I}_{2\times 2} \end{bmatrix}_{4\times 4} \tag{28}$$

$$B_a = \begin{bmatrix} B_{vd} \\ CB_{vd} \end{bmatrix}_{4\times 1} \tag{29}$$

$$C_a = [0_{2\times 2} \ \mathrm{C}]_{2\times 4} \tag{30}$$

The weighting matrices Q and R are chosen as symmetric positive-definite matrices. They are tuning parameters of appropriate dimensions.

3.3. Lower-level steering subsystem PI controller

Based on the BLDC (12) to (14), a linear state space model has been derived in section 2. The steering angle reference δ_{fref} supplied by the AMPC controller is fed to the control scheme. The lower-level PI controller is therefore designed to ensure that the physical steering actuator accurately tracks the steering-angle reference generated by the upper-level vehicle controller.

Let the steering subsystem state $x = [x_1, x_2, x_3]^{\mathrm{T}} = [i, \omega_M, \theta_M]^{\mathrm{T}} \in \mathbb{R}^3$, where θ_M is the BLDC angular position, and the input duty cycle $u = \alpha$. The angular position of the BLDC motor is related to the steering actual angle via an equivalent gear ratio r.

The state space PI control law is expressed as (31) [16]:

$$u = -K_p x - K_i \int \theta_M - \theta_{Mref}\, dt \tag{31}$$

and:

$$\theta_{Mref} = \frac{1}{r}\delta_{fref} \tag{32}$$

The proportional and integral gains K_p and K_i are obtained using the classical pole-placement technique as applied to the augmented system matrix, as described in standard state-space control theory (Brogan [23],

Chen [24]). Similar pole-placement tuning methods have been employed in vehicle lateral stability and steering control applications [25].

3.4. State feedback filtering using the EKF

The Kalman filter was originally formulated for state estimation in linear dynamic systems using noisy sensor measurements. For nonlinear systems, this framework is extended through the Extended Kalman Filter (EKF), which represents the nonlinear dynamics through a local linear approximation about the current estimate through first-order Taylor linearization. This local linearization enables recursive estimation of the system states while accounting for process and measurement uncertainties [26], [27].

In this study, the EKF is implemented using the linearized vehicle model derived from (20) and (21). Let $w \in \mathbb{R}^2$ and $v \in \mathbb{R}^2$ denote the process-noise and measurement-noise vectors, respectively. The nonlinear stochastic system employed for the estimator can therefore be written as (33).

$$\begin{cases} \dot{x} = f\big(x, (u + w)\big) \\ \quad y = x + v \end{cases} \tag{33}$$

The two noise processes are assumed to be independent zero-mean white Gaussian processes, with covariance matrices $Q_n \in \mathbb{R}$ and $R_n \in \mathbb{R}^{2\times2}$, respectively.

The EKF algorithm is formulated as (34)-(38) [1].

$$\hat{x}_0 = E[X_0] \tag{34}$$

$$P(0) = E[(x_0 - \hat{x}_0)(x_0 - \hat{x}_0)^T] \tag{35}$$

$$K = P{R_n}^{-1} \tag{36}$$

$$\dot{\hat{x}} = f\big(\hat{x}, (u + w_0)\big) + K(y - \hat{x}) \tag{37}$$

$$\dot{P} = A_v P + P{A_v}^T + B_v Q_n {B_v}^T - P{R_n}^{-1} P \tag{38}$$

P stands for the estimation-error covariance matrix. Since the noise w is affecting the steering angle directly, matrix A_v is given by (20), and matrix B_v is given by (39).

$$B_v = \begin{pmatrix} \left.\frac{df_1}{dw}\right|_{x_0,u_0} \\ \left.\frac{df_2}{dw}\right|_{x_0,u_0} \end{pmatrix} \tag{39}$$

3.5. MATLAB/Simulink simulation setup

Figure 4 depicts the comprehensive MATLAB/Simulink simulation framework developed to assess the proposed approach. The simulation framework consists of a reference model, an EKF, an AMPC, the BLDC steering actuator, and the nonlinear vehicle model based on the single-track representation. The reference model provides the desired lateral velocity and yaw-rate trajectories from the driver steering command and the longitudinal vehicle speed. To reproduce realistic operating conditions, process and measurement noise are injected into the plant through the noise generation subsystem, which also provides the corresponding covariance matrices used by the EKF. The estimated vehicle states are then supplied to the AMPC controller, while the steering command generated by the controller is tracked by the BLDC actuator before being applied to the nonlinear vehicle model.

The EKF estimates the vehicle states from the noisy measurements and supplies the estimated lateral velocity and yaw rate to the AMPC. Using these estimated states and the reference trajectories, the controller computes the desired steering angle. This steering command is then applied to the inner-loop BLDC motor controller, which accurately tracks the requested steering angle and drives the steering mechanism.

Finally, the computed steering angle is applied to the nonlinear vehicle dynamics based on the Pacejka tire formulation. The resulting vehicle responses are returned to the observer and controller, thereby closing the control loop and enabling the evaluation of the proposed strategy under noisy operating conditions. This feedback interaction allows the effect of the actuator dynamics and state-estimation accuracy on the overall vehicle response to be assessed simultaneously.

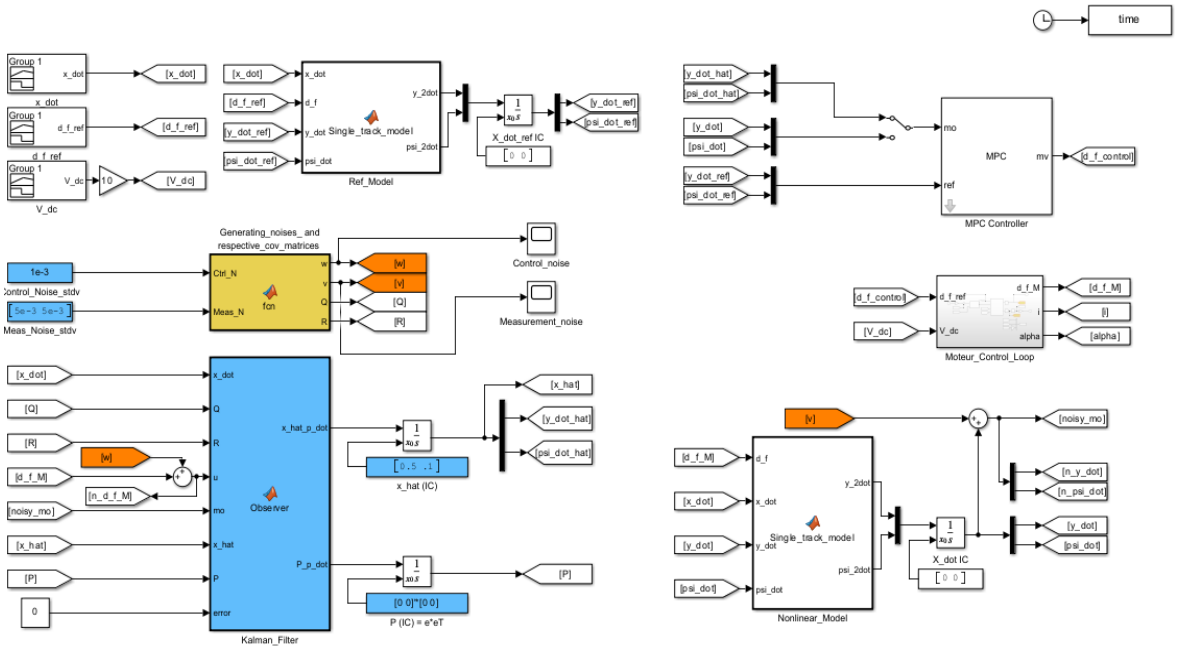

Figure 4. Simulation setup

4. RESULTS AND DISCUSSION

This section assesses the performance of the proposed AMPC framework for the nonlinear vehicle model equipped with a BLDC-actuated steering system and an EKF-based state estimator. The controller effectiveness is investigated through its ability to track the vehicle lateral velocity v_y and yaw rate $\dot{\psi}$. The overall control architecture is presented in Figure 5. All the simulation required parameters are listed in Table 1.

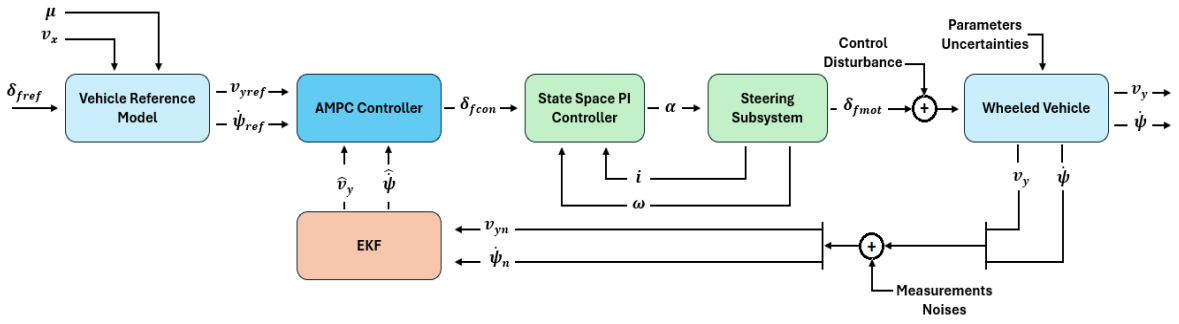

Figure 5. Block diagram of the proposed AMPC–EKF control scheme

Table 1. Numerical parameters of the vehicle, BLDC motor, and controllers

Parameters	Values		
Vehicle	$I_z = 2873\ kg.m^2$	$l_f = 1{,}1\ m$	
	$m = 1573\ kg$	$l_r = 1.58\ m$	
Tire/road		$\mu = 1.1$	
Magic formula	$B = 12.12$	$C = 1.65$	$E = -0.5804$
MPC controller	$N_p = 100$	$N_c = 2$	T_s=10^{-5}
	$R = 0.1$	$Q = diag(1.1)$	
BLDC	p = 1	B = 0.00021	
	J = 0.00098	L = 0.00034	
	K_e = 0.0345	V_{dc} = 48V	
	K_t = 2*p*K_e	R = 0.42	
State feedback controller	M = [1 0 0]	P_{ci} = 1e3*[-2 -2 -2 -2]	

To systematically evaluate the performance of each control layer, three simulation scenarios were considered. First, the outer loop controller is evaluated assuming ideal actuation. Second, the inner loop actuator controller is tested independently. Third, the complete nested control architecture is analyzed. Finally, a Kalman filter-based state estimator is integrated into the nested loop to evaluate robustness against measurement noise.

The vehicle longitudinal velocity is assumed to be externally prescribed and varies over time according to a predefined profile. Two reference driving maneuvers, namely the SLC and the DLC, are defined in terms of lateral road trajectories. The corresponding steering reference profiles required to follow these maneuvers are subsequently derived and employed within the control framework. Figures 6 and 7 illustrate the longitudinal velocity and reference steering angle profiles used.

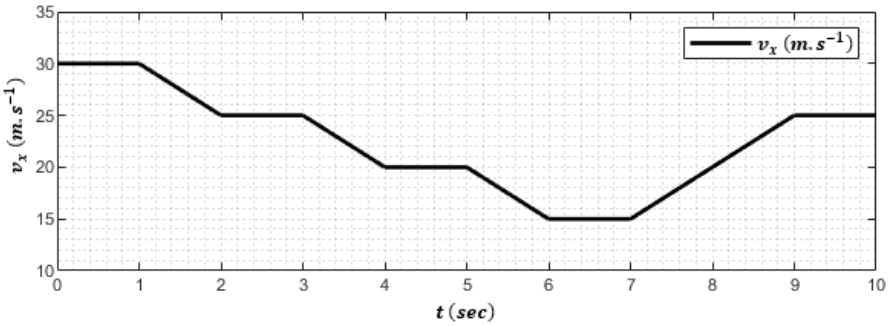

Figure 6. Vehicle longitudinal speed

4.1. Upper-level control loop using AMPC controller

In a first stage, the AMPC controller is tested using a nonlinear vehicle model with the parameters reported by Table 1. Local linearization is performed to obtain the matrices required by the AMPC formulation. In this scenario, an ideal steering actuator is assumed and full state information is considered available, allowing the intrinsic performance of the AMPC strategy to be isolated and thus validated. Despite the challenging longitudinal speed and reference steering angle profiles, the controller ensures stable and well-behaved lateral velocity and yaw rate responses as shown in Figures 8 and 9.

To quantitatively assess the tracking performance, the metrics reported in Table 2 are evaluated. The lateral error RMSE and maximum lateral error confirm the high trajectory-tracking accuracy observed in the figures, while the heading error metrics indicate satisfactory yaw-angle regulation. Furthermore, the overshoot value provide insight into the transient behavior of the closed-loop system and its ability to rapidly converge to the desired lane position.

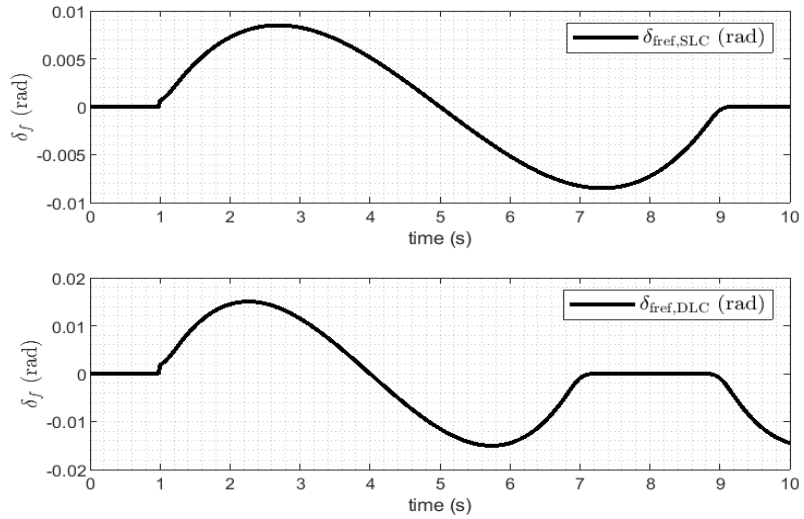

Figure 7. Reference steering angle profiles

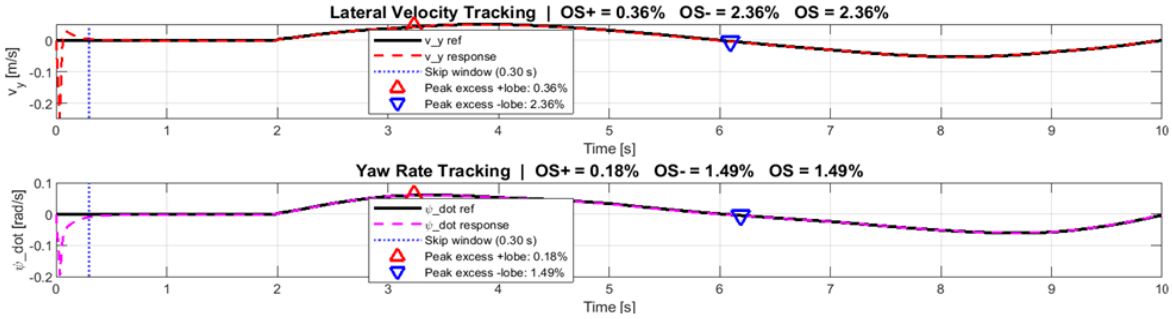

Figure 8. Lateral velocity and yaw rate of the vehicle considering SLC profile for Scenario 1

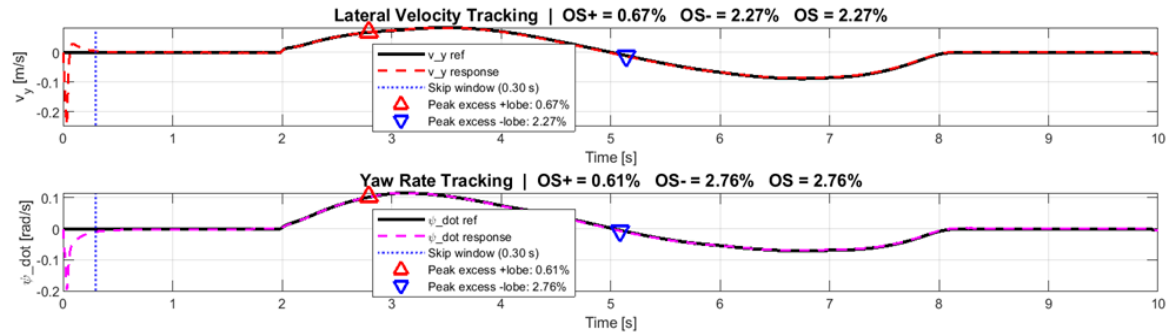

Figure 9. Lateral velocity and yaw rate of the vehicle considering DLC profile for Scenario 1

Table 2. Performance metric for Scenario 1

Performance metric	SLC	DLC
Lateral error RMSE (m)	0.005812	0.004726
Maximum lateral error (m)	0.007421	0.007305
Steady-state lateral deviation (m)	0.007159	0.003278
Heading error RMSE (rad/s)	0.010945	0.011421
Maximum heading error (rad/s)	0.197676	0.247143
Overshoot (%)	2.36	2.27

4.2. Nested loop

In this section, the BLDC motor control loop based on a pole placement state-space feedback control is integrated into the AMPC-based vehicle control framework previously evaluated. The resulting nested control architecture consists of the AMPC outer loop generating steering commands, which are subsequently tracked by the BLDC motor inner loop. The reference maneuver constitutes the input of the overall simulation system. The effectiveness of the state-space feedback controller is evaluated for both previously defined maneuvers, namely the single lane change (SLC) and double lane change (DLC) trajectories. The outputs of interest include the motor angular position associated with the inner loop, the current of the BLDC motor as well as the vehicle lateral velocity and yaw angle associated with the outer loop. Figure 10 presents the tracking response of the controller to the AMPC controller steering angle $\delta_{fcontrol}$. Similar tracking behavior is obtained for both SLC and DLC maneuvers. The simulation result demonstrates very fast tracking of the angular position from the beginning and during all the simulation duration. In particular, the accurate tracking obtained for the DLC profile, which represents a more aggressive maneuver, further demonstrates the effectiveness of the proposed control strategy. Figure 11 illustrates the BLDC motor phase current while Figure 12 presents the corresponding duty cycle applied to the motor for both SLC and DLC maneuvers.

After a short transient at the beginning of the simulation, it can be observed that, both signals remain continuous and bounded throughout the maneuver. Similar responses are observed for the two trajectories, indicating feasible actuator operation even under the more aggressive DLC maneuver. This behavior indicates that the inner-loop controller maintains the actuator variables within bounded operating conditions while following the steering commands generated by the AMPC.

For the AMPC control outer loop, commonly used sensors, as accelerometers and gyroscopes, may provide lateral speed and yaw rate. In this section, those measurements are supposed to be available. The AMPC controller tracking results are illustrated in Figures 13 and 14. Once again, the control signal is optimized to ensure very satisfying tracking abilities from the beginning of the driver steering scenarios and during all its different phases. The vehicle lateral dynamic variables are stable even under vehicle longitudinal speed changing and in spite of the challenging driving maneuver profiles.

Table 3 summarizes the performance metrics obtained in Scenario 2, where the complete cascaded control architecture, including the outer-loop path-following controller and the inner-loop BLDC motor steering actuator, is evaluated under both SLC and DLC maneuvers. The selected metrics assess the tracking accuracy of the outer loop in terms of lateral and heading errors, as well as the dynamic performance of the steering actuator through steering-angle tracking error, rise time, and settling time. These indicators offer a comprehensive assessment of the effectiveness of the integrated control system in ensuring accurate trajectory tracking and rapid actuator response.

The obtained results show that the proposed architecture provides accurate path tracking for both maneuvers. The outer-loop controller maintains very low lateral tracking errors, with lateral-error RMSE values below 6 mm and maximum lateral deviations below 8 mm, indicating highly accurate adherence to the reference trajectory. Similarly, the heading-error RMSE remains close to 0.011 rad for both scenarios, while the maximum heading error is limited to approximately 0.198 rad, confirming satisfactory vehicle orientation tracking throughout the maneuvers. The overshoot remains low in both cases (2.36% for SLC and 2.27% for DLC), highlighting a stable and well-damped response. Regarding the steering actuator, the inner-loop controller exhibits identical performance in both maneuvers, achieving a steering-angle RMSE of 0.004667 rad, with a rise time of 0.3 ms, together with a settling time of 37.2 ms. These results indicate that the BLDC actuator dynamics are significantly faster than the vehicle dynamics, enabling the actuator to accurately and promptly follow steering commands generated by the outer-loop controller without degrading the overall path-following performance.

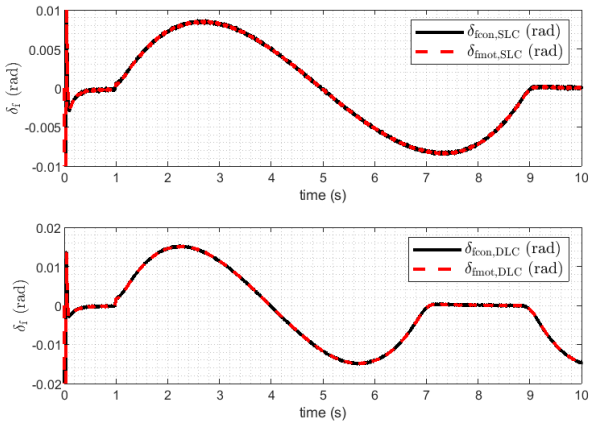

Figure 10. Reference steering angle & BLDC rotor position

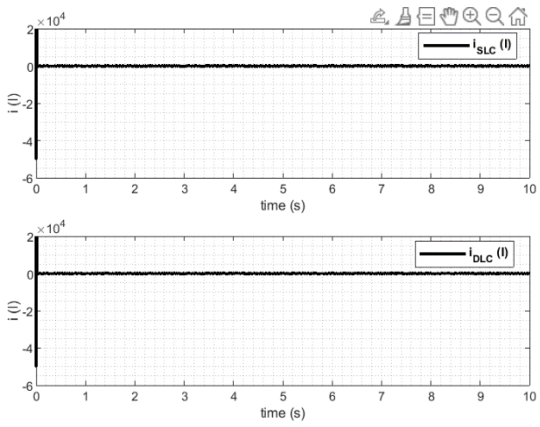

Figure 11. Phase current of the BLDC motor

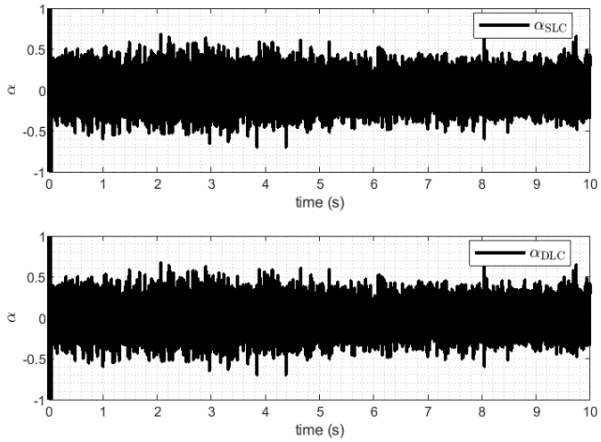

Figure 12. Duty cycle of the BLDC motor

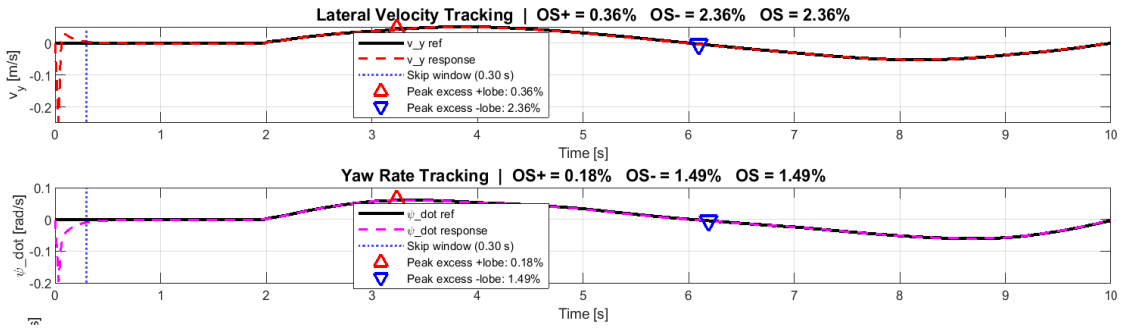

Figure 13. Vehicle lateral velocity and yaw rate under the SLC profile for Scenario 2

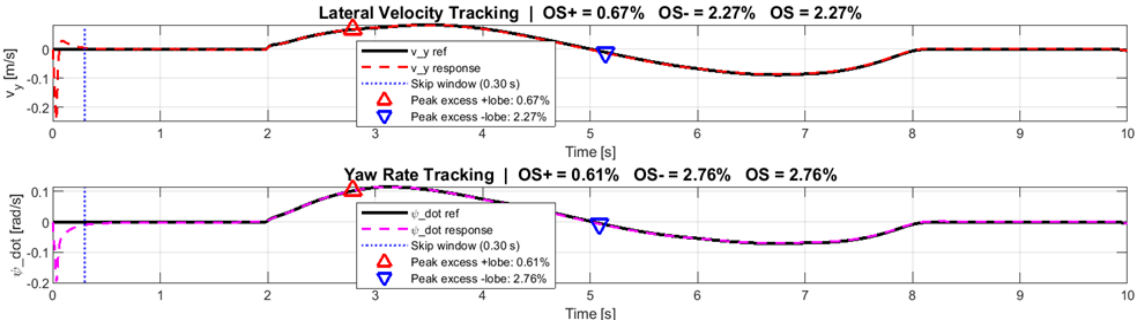

Figure 14. Vehicle lateral velocity and yaw rate under the DLC profile for Scenario 2

Table 3. Performance metric for Scenario 2

Performance metric		SLC	DLC
Outer loop	Lateral error RMSE (m)	0.005812	0.004726
	Maximum lateral error (m)	0.007421	0.007305
	Steady-state lateral deviation (m)	0.007159	0.003278
	Heading error RMSE (rad)	0.010945	0.010976
	Maximum heading error (rad)	0.197676	0.197676
	Overshoot (%)	2.36	2.27
Actuator performance (inner loop — BLDC motor)	Steering angle tracking RMSE (rad)	0.004667	0.004667
	Maximum steering angle error (rad)	0.384771	0.384771
	Rise time (s)	0.0003	0.0003
	Settling time (s)	0.0372	0.0372

4.3. Control strategy assessment under input disturbance and measurement noise

In this scenario, the EKF is used to tackle an external bounded disturbance on the steering angle and Gaussian white noises affecting the available outputs. This scenario is introduced to evaluate the robustness of the complete control architecture under simultaneous actuator disturbances and measurement uncertainty. The estimated states are then supplied to the AMPC controller to assess whether accurate tracking can be maintained despite these uncertainties

Figure 15 shows, respectively the noisy lateral velocity and yaw rate applied to update the state estimate alongside with their respective estimates for the SLC maneuver. The EKF is employed to provide accurate state estimates (lateral velocity and yaw rate) in the presence of Gaussian measurement noise. Beyond conventional implementations, the EKF is integrated within a nested control architecture that includes a BLDC motor-driven steering actuator. This configuration enables the estimator to account not only for nonlinear vehicle dynamics but also for disturbances and uncertainties arising from the actuator and its power electronics-based control, such as duty-cycle-induced perturbations and actuator dynamics. By improving the reliability of the state feedback supplied to the AMPC controller, the EKF improves the overall robustness and stability of the control architecture under realistic operating conditions. Similar estimation accuracy is obtained for the more aggressive DLC maneuver, as shown in Figure 16.

As illustrated in Figure 17, the EKF based AMPC tracking abilities are highly accurate. Despite the noise present in the control input and the available outputs, the controller successfully followed the driver reference vehicle behavior in the presence of longitudinal speed variations. Under the more severe DLC

maneuver combined with disturbances, the controller demonstrates consistently strong robustness. As demonstrated in Figure 18, The lateral states remain bounded, and no instability is observed.

Overall, the EKF tuning is very suitable for the AMPC controller, and the control strategy is quite insensitive to the steering disturbance as well as the output noises. Table 4 presents the performance evaluation results for Scenario 3, which incorporates the complete autonomous steering system, including the outer-loop path-following controller, the inner-loop BLDC motor actuator, and the Kalman filter-based state estimator. The system is assessed under SLC and DLC maneuvers using tracking, transient-response, actuator-performance, and state-estimation metrics. This comprehensive evaluation enables the analysis of both control accuracy and estimation quality, thereby providing insight into the effectiveness of the integrated control and observation framework.

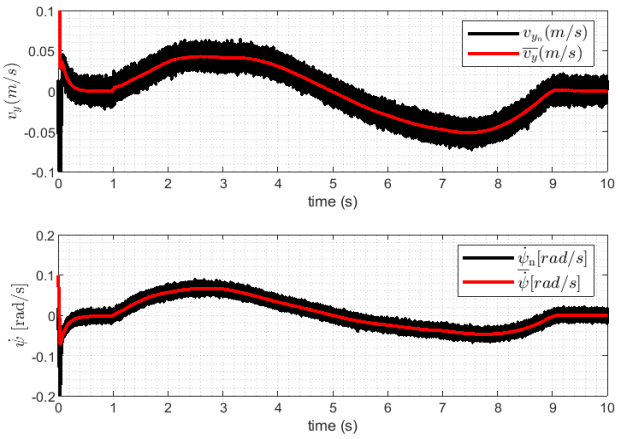

Figure 15. Estimated and noisy lateral velocity and yaw-rate outputs under the DLC profile

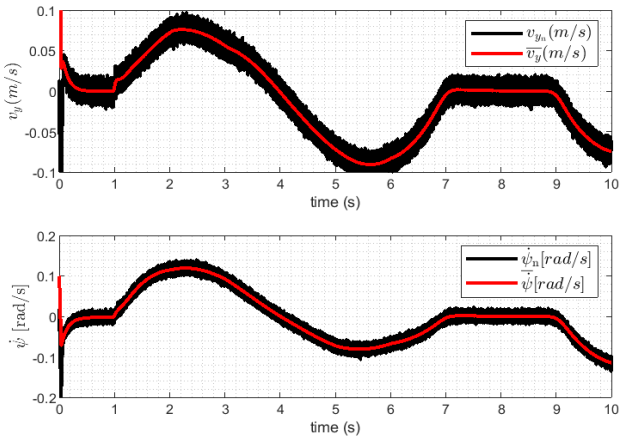

Figure 16. Estimated and noisy lateral velocity and yaw-rate outputs under the DLC profile

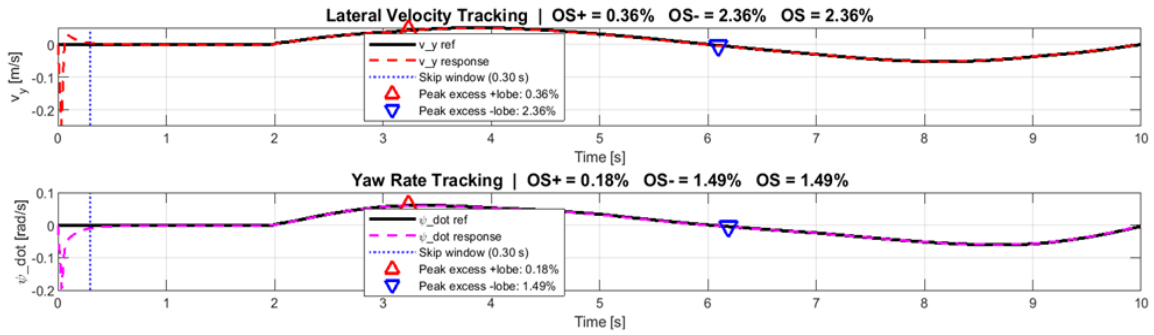

Figure 17. Lateral velocity and yaw rate for noisy inputs and SLC profile for Scenario 3

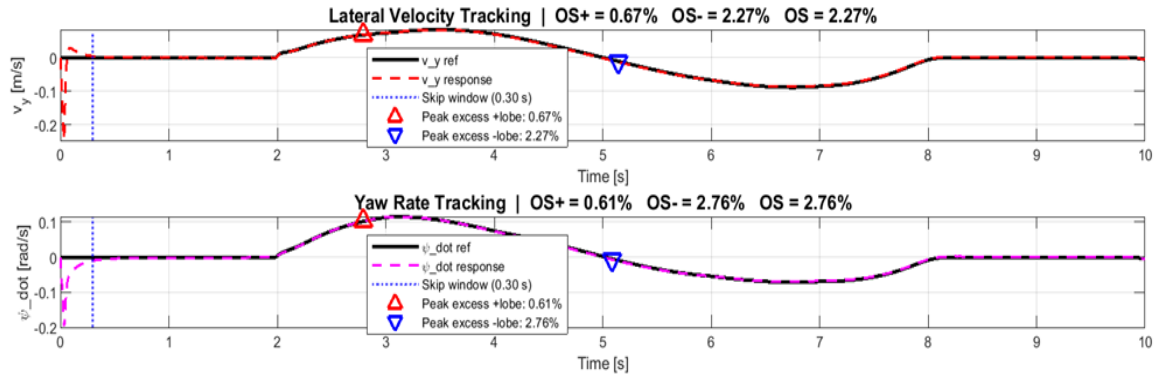

Figure 18. Lateral velocity and yaw rate for noisy inputs and DLC profile for Scenario 3

Table 4. Performance metric for Scenario 3

Performance metric		SLC	DLC
Outer loop	Lateral error RMSE (m)	0.005812	0.004726
	Maximum lateral error (m)	0.007421	0.007305
	Steady-state lateral deviation (m)	0.007159	0.003278
	Heading error RMSE (rad)	0.010945	0.010976
	Maximum heading error (rad)	0.197676	0.197676
	Overshoot (%)	2.36	2.27
Actuator performance	Steering angle tracking RMSE (rad)	0.004667	0.004667
(inner loop)	Maximum steering angle error (rad)	0.384771	0.384771
State estimation quality	Lateral position estimation RMSE (m)	0.017507	0.017504
(Kalman Filter)	Yaw rate estimation RMSE (rad/s)	0.008285	0.008285
	Lateral velocity estimation RMSE (m/s)	0.024544	0.024544

The results indicate that the proposed controller preserves accurate path tracking despite the inclusion of estimated states in the feedback loop. For both SLC and DLC maneuvers, the lateral-error RMSE remains below 6 mm, while the maximum lateral deviation does not exceed 8 mm, demonstrating precise trajectory tracking. Likewise, the heading-error RMSE is approximately 0.011 rad, with a maximum heading error of 0.198 rad, confirming accurate orientation control throughout the maneuvers. The transient-response metrics reveal a stable behavior characterized by low overshoot values of 2.36% and 2.27% for SLC and DLC, respectively, while the DLC maneuver exhibits a faster settling time (8.44 s) compared with the SLC case (10 s). The actuator-performance results show identical behavior in both maneuvers, with a steering-angle tracking RMSE of 0.004667 rad and a maximum steering-angle error of 0.384771 rad, indicating that the BLDC motor accurately follows the steering commands generated by the outer-loop controller. Furthermore, the Kalman filter provides reliable state estimates, achieving low estimation errors for lateral position (≈0.0175 m), yaw rate (≈0.0083 rad/s), and lateral velocity (≈0.0245 m/s). These results confirm that the proposed observer is capable of accurately reconstructing the vehicle states required for feedback control, thereby preserving the overall tracking performance while reducing dependence on direct state measurements.

To assess the performance of the proposed control architecture, Table 5 presents a comprehensive comparison of the key performance metrics obtained from simulation across the three control scenarios and both lane-change maneuvers. The evaluated metrics cover lateral tracking accuracy, heading deviation, steady-state residual error, and transient response quality, providing a complete picture of the system behavior from the ideal actuation case through to the full nested control scheme with Kalman state estimation.

Table 5. Comparison of the key performance metrics

Performance metric	Scenario 1 - Ideal actuation		Scenario 2 - Nested (AMPC+BLDC)		Scenario 3 - Nested + Kalman	
	SLC	DLC	SLC	DLC	SLC	DLC
Lateral error RMSE (m)	0.005812	0.004726	0.005812	0.004726	0.005812	0.004726
Peak lateral deviation (m)	0.007421	0.007305	0.007421	0.007305	0.007421	0.007305
Steady-state lateral deviation (m)	0.007159	0.003278	0.007159	0.003278	0.007159	0.003278
Heading error RMSE (rad)	0.010945	0.011421	0.010945	0.010976	0.010945	0.010976
Maximum heading deviation (rad)	0.197676	0.247143	0.197676	0.197676	0.197676	0.197676
Overshoot (%)	2.36	2.27	2.36	2.27	2.36	2.27

The results presented in Table 5 show that the three simulation scenarios exhibit nearly identical tracking performance. This behavior is expected because each scenario evaluates a different level of implementation of the proposed control architecture, from ideal steering actuation to realistic steering dynamics and noisy measurements. Scenario 1 establishes the baseline performance of the proposed AMPC under ideal steering actuation. Scenario 2 replaces the ideal steering input with the BLDC steering subsystem controlled by the state-space PI controller. The nearly unchanged tracking metrics, with lateral error RMSE and maximum lateral error remaining at 0.0058 m and 0.0075 m for SLC and 0.0047 m and 0.0073 m for DLC, respectively, indicate that the steering subsystem accurately reproduces the steering commands generated by the AMPC without noticeable degradation in tracking performance. Scenario 3 further incorporates the EKF for estimating vehicle states under measurement noise. The negligible differences in the performance metrics demonstrate that the EKF provides sufficiently accurate state estimates for the AMPC, enabling the controller to maintain its tracking accuracy under realistic sensing conditions. A lower steady-state lateral error is observed in DLC than in SLC, which can be attributed to the symmetric return phase of the double lane change. Although the overall tracking performance remains nearly unchanged, the maximum heading error in DLC decreases from 0.248 rad in Scenario 1 to 0.198 rad in Scenarios 2 and 3, indicating a smoother yaw response with the closed-loop steering dynamics. The overshoot also remains stable at 2.36% for SLC and 2.27% for DLC across all scenarios. These observations highlight the specific contribution of each component within the proposed architecture: the AMPC is primarily responsible for path tracking, the state-space PI controller and brushless direct current (BLDC) subsystem ensure accurate steering actuation under realistic dynamics, and the EKF provides reliable state estimates in the presence of measurement noise. Overall, the results confirm the modularity and robustness of the proposed nested architecture while preserving the tracking performance established under ideal conditions.

To further validate the proposed approach against existing literature, Table 6 presents a side-by-side comparison between the AMPC–BLDC–EKF architecture developed in this work and the AMPC scheme reported in [26], evaluated under the double lane change maneuver at 10, 15, and 19 m/s, in terms of lateral position RMSE (e_y) and yaw angle RMSE (e_φ). The proposed system reduces lateral tracking error by 82–93% and yaw angle error by 67–73% across the three speeds, with both gains widening as speed increases. Notably, while the benchmark's lateral error grows with speed (0.08 → 0.16 m), the proposed system's error slightly decreases instead (0.0144 → 0.0117 m), indicating that the nested AMPC–BLDC control loop, corrected by the Kalman-filtered feedback, keeps tracking stable even under real actuator dynamics as the maneuver becomes more demanding.

Table 6. Performance comparison with the AMPC scheme reported in [26]

Speed	e_y (Lateral position RMSE)			e_φ (Yaw angle RMSE)		
	Ref. AMPC (m)	Proposed (m)	Gain (%)	Ref. AMPC (deg)	Proposed (deg)	Gain (%)
10 m/s	0.08	0.0144	82.0%	1.86	0.577	69.0%
15 m/s	0.10	0.0131	86.9%	1.85	0.604	67.4%
19 m/s	0.16	0.0117	92.7%	2.35	0.644	72.6%

5. CONCLUSION

This paper has developed and evaluated, in MATLAB/Simulink, a hierarchical AMPC-BLDC-EKF architecture for improving the lateral stability for a nonlinear vehicle fitted with a BLDC-actuated steer-by-wire system. It combines an AMPC for vehicle-level path tracking, a state-space PI controller for steering actuation, and an EKF for state estimation under noisy measurements. Simulation results obtained during single lane change (SLC) and double lane change (DLC) maneuvers demonstrated accurate tracking of the lateral vehicle states under varying longitudinal velocity and road adhesion conditions. The incorporation of the BLDC steering subsystem preserved the tracking performance achieved by the AMPC, while the EKF provided reliable state estimates that maintained controller performance under measurement noise and bounded disturbances in the steering input. The obtained results confirm the effectiveness and robustness of the proposed architecture under the considered simulation conditions, suggesting its potential for future application in cost-effective electric vehicle steering systems, subject to additional hardware-in-the-loop and experimental validation. The current investigation is restricted to MATLAB/Simulink-based simulations. Future investigations will address hardware-in-the-loop testing and experimental validation of the proposed architecture, together with the inclusion of longitudinal load transfer, combined tire slip, and braking dynamics to improve the fidelity of the vehicle model. In addition, sensitivity analyses of the AMPC and EKF tuning parameters will be conducted to further evaluate the robustness and applicability of the proposed control strategy under a wider range of operating conditions.

FUNDING INFORMATION

Authors state no funding involved.

AUTHOR CONTRIBUTIONS STATEMENT

This journal uses the Contributor Roles Taxonomy (CRediT) to recognize individual author contributions, reduce authorship disputes, and facilitate collaboration.

Name of Author	C	M	So	Va	Fo	I	R	D	O	E	Vi	Su	P	Fu
Fatima-Zahra Rahmouni	✓	✓	✓		✓	✓	✓	✓	✓	✓			✓	
Mohammed Bakhti	✓	✓		✓		✓		✓	✓	✓	✓	✓		

C : **C**onceptualization
M : **M**ethodology
So : **So**ftware
Va : **Va**lidation
Fo: **Fo**rmal analysis
I : **I**nvestigation
R : **R**esources
D : **D**ata Curation
O : Writing - **O**riginal Draft
E : Writing - Review & **E**diting
Vi : **Vi**sualization
Su : **Su**pervision
P : **P**roject administration
Fu : **Fu**nding acquisition

CONFLICT OF INTEREST STATEMENT

Authors state no conflict of interest.

DATA AVAILABILITY

Data availability is not applicable to this paper as no new data were created or analyzed in this study.

REFERENCES

[1] N. Zhang *et al.*, "A state-of-the-art review on the revolution of structure and control of vehicle chassis system: from tradition to distributed chassis system," *Chinese Journal of Mechanical Engineering (English Edition)*, vol. 38, no. 1, 2025, doi: 10.1186/s10033-025-01297-5.

[2] B. Leng, W. Han, S. Solmaz, R. John, and L. Xiong, "Modeling, analysis and control on vehicle lateral dynamics with chassis heterogeneous actuators," *Chinese Journal of Mechanical Engineering (English Edition)*, vol. 38, no. 1, 2025, doi: 10.1186/s10033-025-01345-0.

[3] D. Tavella, J. Tolkacz, B. Wasacz, D. Peraboni, and R. Corradi, "Cross-domain control architecture - single master controller for propulsion and chassis automotive domains," in *SAE Technical Papers*, SAE International, Mar. 2022, doi: 10.4271/2022-01-0746.

[4] M. A. P. Perdana *et al.*, "Control strategies for steer-by-wire systems: an overview," *Technologies*, vol. 13, no. 1, 2025, doi: 10.3390/technologies13010006.

[5] Y. Hu, X. Ji, K. Chen, and X. Ma, "Elementary study on BLDC controller for electric power steering system," in *SAE 2004 World Congress & Exhibition*, Mar. 2004, doi: 10.4271/2004-01-1096.

[6] H. Adibi-Asl, A. Doosthosseini, and A. Taghavipour, "Using adaptive pole placement control strategy for active steering safety system," *International Journal of Industrial and Manufacturing Engineering*, vol. 11, no. 3, pp. 524–528, 2017, doi: 10.5281/zenodo.1129145.

[7] M. Thompson, J. Dallas, J. Y. M. Goh, and A. Balachandran, "Adaptive nonlinear model predictive control: maximizing tire force and obstacle avoidance in autonomous vehicles," *IEEE Transactions on Field Robotics*, vol. 1, pp. 318–331, 2024, doi: 10.1109/tfr.2024.3497925.

[8] E. A. Teklu and C. M. Abdissa, "Genetic algorithm tuned super twisting sliding mode controller for suspension of maglev train with flexible track," *IEEE Access*, vol. 11, pp. 30955–30969, 2023, doi: 10.1109/ACCESS.2023.3262416.

[9] L. Alfeqy, H. E. H. Abdelmunim, S. A. Maged, and D. Emad, "Kalman filter-based fusion of lidar and camera data in bird's eye view for multi-object tracking in autonomous vehicles," *Sensors*, vol. 24, no. 23, 2024, doi: 10.3390/s24237718.

[10] B. Duan, "Sensor and sensor fusion technology in autonomous vehicles," *Applied and Computational Engineering*, vol. 52, no. 1, pp. 132–137, 2024, doi: 10.54254/2755-2721/52/20241470.

[11] G. Reina and A. Messina, "Vehicle dynamics estimation via augmented extended Kalman filtering," *Measurement: Journal of the International Measurement Confederation*, vol. 133, pp. 383–395, 2019, doi: 10.1016/j.measurement.2018.10.030.

[12] A. T. Nguyen, L. Frezzatto, T. M. Guerra, and S. Delprat, "Cost-effective estimation of vehicle lateral tire-road forces and sideslip angle via nonlinear sampled-data observers: theory and experiments," *IEEE/ASME Transactions on Mechatronics*, vol. 29, no. 6, pp. 4606–4617, 2024, doi: 10.1109/TMECH.2024.3382777.

[13] J. Sterthoff, R. Henze, and F. Küçükay, "Vehicle handling improvements through Steer-by-Wire," *Automotive and Engine Technology*, vol. 6, no. 1–2, pp. 91–98, Jun. 2021, doi: 10.1007/s41104-021-00079-0.

[14] R. Rajamani, *Vehicle Dynamics and controls*. Springer New York Dordrecht Heidelberg London, 2012.

[15] H. B. Pacejka, *Tire and vehicle dynamics, third edition*, 3rd ed. Elsevier, 2012, doi: 10.1016/C2010-0-68548-8.

[16] C. L. Xia, *Permanent magnet brushless DC motor drives and controls*, John Wiley & Sons, 2012.

[17] B. Li, H. Du, W. Li, and B. Zhang, "Non-linear tyre model–based non-singular terminal sliding mode observer for vehicle velocity and side-slip angle estimation," *Proceedings of the Institution of Mechanical Engineers, Part D: Journal of Automobile Engineering*, vol. 233, no. 1, pp. 38–54, 2019, doi: 10.1177/0954407018788720.

[18] K. B. Singh, M. A. Arat, and S. Taheri, "An intelligent tire based tire-road friction estimation technique and adaptive wheel slip controller for antilock brake system," *Journal of Dynamic Systems, Measurement and Control, Transactions of the ASME*, vol. 135, no. 3, 2013, doi: 10.1115/1.4007704.
[19] H. Guo, D. Cao, H. Chen, C. Lv, H. Wang, and S. Yang, "Vehicle dynamic state estimation: state of the art schemes and perspectives," *IEEE/CAA Journal of Automatica Sinica*, vol. 5, no. 2, pp. 418–431, 2018, doi: 10.1109/JAS.2017.7510811.
[20] H. Dugoff, P. S. Fancher, and L. Segel, "An analysis of tire traction properties and their influence on vehicle dynamic performance," in *SAE Technical Papers*, SAE International, 1970, pp. 341–366, doi: 10.4271/700377.
[21] H. Lee and S. Taheri, "Intelligent tires-a review of tire characterization literature," *IEEE Intelligent Transportation Systems Magazine*, vol. 9, no. 2, pp. 114–135, 2017, doi: 10.1109/MITS.2017.2666584.
[22] L. Wang, "A tutorial on model predictive control: using a linear velocity-form model," *Developments in Chemical Engineering and Mineral Processing*, vol. 12, no. 5–6, pp. 573–614, Jan. 2004, doi: 10.1002/apj.5500120511.
[23] W. L. Brogan, *Modern Control Theory*. Prentice Hall, 1991.
[24] C. T. Chen, *Linear system theory and design*, 4th ed. Oxford University Press, 2012.
[25] G. L. Plett, "Extended kalman filtering for battery management systems of LiPB-based HEV battery packs - part 1. background," *Journal of Power Sources*, vol. 134, no. 2, pp. 252–261, 2004, doi: 10.1016/j.jpowsour.2004.02.031.
[26] M. Doumiati, A. Charara, A. Victorino, D. Lechner, and B. Dubuisson, *Vehicle dynamics estimation using Kalman filtering: experimental validation*. ISTE Ltd. and John Wiley & Sons, 2013.
[27] J. M. Guirguis, S. Hammad, and S. A. Maged, "Path tracking control based on an adaptive MPC to changing vehicle dynamics," *International Journal of Mechanical Engineering and Robotics Research*, vol. 11, no. 7, pp. 535–541, 2022, doi: 10.18178/ijmerr.11.7.535-541.

BIOGRAPHIES OF AUTHORS

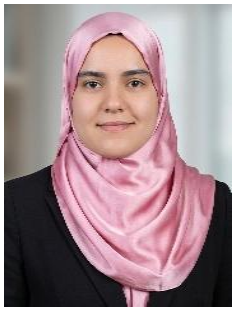

Fatima Zahra Rahmouni is a Ph.D. candidate in control systems at Moulay Ismail University in Meknes, Morocco. She graduated as an Electromechanical and Industrial Systems Engineer from ENSAM Meknes. She has over six years of experience as a product engineer in the automotive industry. Her research focuses on nonlinear control, vehicle dynamics, and advanced control techniques for electric drive systems. She has contributed to international conferences and co-authored two conference papers. She can be contacted at email: f.rahmouni@edu.umi.ac.ma.



Mohammed Bakhti is a professor specializing in supervision, monitoring, and control systems at Moulay Ismail University in Meknes, Morocco. His research interests include the control, observation, and identification of both linear and nonlinear systems. He has published more than 24 articles in peer-reviewed journals and also serves as a reviewer for several international scientific journals. He holsds a Ph.D. in active vibration control of flexible manipulators from Moulay Ismail University in Meknes, Morocco. He can be contacted at email: m.bakhti@umi.ac.ma.